JOURNAL OF GEOPHYSICAL RESEARCH, VOL. 115, A06201, doi:10.1029/2009JA015119, 2010

Saturation of transpolar potential for large *Y* component interplanetary magnetic field

E. J. Mitchell,[1] R. E. Lopez,[1] R. J. Bruntz,[1] M. Wiltberger,[2] J. G. Lyon,[3] R. C. Allen,[1] S. J. Cockrell,[1] and P. L. Whittlesey[1]

Received 19 November 2009; revised 13 January 2010; accepted 15 January 2010; published 3 June 2010.

[1] This study examines the response of the transpolar potential to a large Y component interplanetary magnetic field (IMF B_y). The transpolar potential responds nonlinearly and saturates for large IMF B_y in the Lyon-Fedder-Mobarry (LFM) global MHD simulation, just as it does for large southward IMF ($-B_z$). Data from Defense Meteorological Satellite Program (DMSP) satellites and Assimilative Mapping of Ionospheric Electrodynamics (AMIE) results confirm the saturation of the transpolar potential during large IMF B_y. The magnitude of the saturated transpolar potential is significantly smaller for large IMF B_y than for large negative IMF B_z. This indicates that transpolar potential saturation does not depend on the strength of the Region 1 current. However, the magnitude of the IMF at which the transpolar potential becomes nonlinear and begins to exhibit saturation behavior is the same for large B_y as it is for large B_z. Furthermore, when the IMF (B_y or B_z) reaches the value that produces saturation, the magnetosheath becomes magnetically dominated, with $\beta < 1$. This suggests that the saturation of the transpolar potential is related to a change in the force balance in the magnetosheath from a plasma-pressure-dominated magnetosheath to a magnetically-dominated magnetosheath.

Citation: Mitchell, E. J., R. E. Lopez, R. J. Bruntz, M. Wiltberger, J. G. Lyon, R. C. Allen, S. J. Cockrell, and P. L. Whittlesey (2010), Saturation of transpolar potential for large *Y* component interplanetary magnetic field, *J. Geophys. Res.*, *115*, A06201, doi:10.1029/2009JA015119.

1. Introduction

[2] The transpolar potential is generated by plasma convection in the polar cap. Polar cap plasma convection is generated through stresses communicated by the solar wind interacting with the magnetosphere-ionosphere system. Two solar wind-magnetosphere-ionosphere interactions are recognized as the source of the ionospheric convection: viscous interaction and dayside merging [*Cowley*, 1982].

[3] Viscous interaction [*Axford and Hines*, 1961] generates ionospheric plasma convection on closed field lines via the transfer of solar wind momentum across the magnetopause to magnetospheric plasma. This generates antisunward plasma convection on closed field lines along the magnetopause and a return sunward flow deeper in the magnetosphere. The convection flow is mirrored in the ionospheric plasma as the magnetospheric stress is communicated on the field lines threading the flow, generating ionospheric electric fields. *Newell et al.* [2008], on the basis of a multiparameter study of magnetospheric state variables, concluded that the amount of viscous-generated transpolar potential is best represented by a factor proportional to the square of the solar wind speed (V) and the square root of the solar wind density (n). A velocity-squared dependence was also suggested by *Boyle et al.* [1997]. The viscous interaction generates approximately 20–30 kV across the ionosphere for normal solar wind conditions [*Reiff et al.*, 1981; *Cowley*, 1982; *Boyle et al.*, 1997; *Sonnerup et al.*, 2001; *Newell et al.*, 2008].

[4] Dayside merging generates ionospheric plasma convection on open field lines [*Dungey*, 1961]. When the interplanetary magnetic field (IMF) is southward, the solar wind magnetic field merges with the magnetospheric field. The solar wind plasma flow draws the merged fields antisunward over the polar cap. The ionospheric plasma attached to the open field lines is also drawn antisunward. When the open field lines reconnect in the tail, the return flow occurs at lower latitudes. This creates the classic two cell convection pattern in the ionosphere. For dawn-dusk IMF orientations, dayside merging creates lopsided convection patterns [*Heppner*, 1977]. For exclusively southward IMF, the ionospheric potential generated by the dayside merging is equal to the projection of the interplanetary electric field (IEF = $-VB_z$) on the extent of the flow

[1]Department of Physics, University of Texas at Arlington, Arlington, Texas, USA.
[2]High Altitude Observatory, National Center for Atmospheric Research, Boulder, Colorado, USA.
[3]Department of Physics and Astronomy, Dartmouth College, Hanover, New Hampshire, USA.

0148-0227/10/2009JA015119

that intersects the dayside merging line [*Burke et al.*, 1999; *Lopez et al.*, 2009]. For an IMF at an arbitrary clock angle (θ), one expects an additional $\sin^2(\theta/2)$ dependence of the potential [*Kan and Lee*, 1979; *Hu et al.*, 2009]. Dayside merging may produce up to 200 kV of the total transpolar potential [*Reiff and Luhmann*, 1986; *Boyle et al.*, 1997; *Hairston et al.*, 2003; *Ober et al.*, 2003].

[5] Thus, the total transpolar potential (the sum of potential produced by viscous interaction and dayside merging) varies with the magnitude and clock angle of the IMF, solar wind speed, and density [*Kan and Lee*, 1979; *Reiff et al.*, 1981; *Cowley*, 1982; *Reiff and Luhmann*, 1986; *Boyle et al.*, 1997; *Sonnerup et al.*, 2001; *Hairston et al.*, 2003; *Ober et al.*, 2003; *Lopez et al.*, 2004; *Newell et al.*, 2008; *Hu et al.*, 2009]. For low values of southward IMF and solar wind speed, the transpolar potential responds linearly to increases in the IMF (R. E. Lopez et al., The role of magnetosheath force balance in regulating the dayside reconnection potential, submitted to *Journal of Geophysical Research*, 2009, and references therein). For larger values of IMF, the extrapolated linear transpolar potential overpredicts the observations; the transpolar potential saturates [*Russell et al.*, 2001; *Siscoe et al.*, 2002a, 2002b; *Ridley*, 2007; *Kivelson and Ridley*, 2008; *Lopez et al.*, 2009]. Transpolar potential saturation is currently explained by three models: the Region 1 current (R1) model [*Siscoe et al.*, 2002a, 2002b], the Alfvén wing (AW) model [*Ridley*, 2007; *Kivelson and Ridley*, 2008], and the magnetosheath force balance (MFB) model (Lopez et al., submitted manuscript, 2009).

[6] The Region 1 current (R1) model suggests the dayside merging portion of transpolar potential (reconnection potential) saturates, because the R1 current reduces the dayside magnetic field [*Siscoe et al.*, 2002a, 2002b]. This reduction limits the rate of dayside merging. If the merging rate is limited, then the reconnection potential is limited. *Siscoe et al.* [2002b] further suggest that the R1 current closes on the bow shock. This R1/bow shock current replaces the Chapman-Ferraro current in balancing the pressure of the solar wind on the magnetosphere. The magnitude of the R1 current is limited to the amount necessary to balance the solar wind. Thus, the amount of current in the system cannot exceed the value needed to stand off the solar wind, and the reconnection potential will saturate at the value needed to supply the required current. Via Ohm's law, the amount of current is proportional to the product of the reconnection potential and the conductivity of the ionosphere. Thus, for the R1 model to be valid, the reconnection potential must saturate at the same value for any given IEF if the conductivity and the solar wind dynamic pressure are constant.

[7] The Alfvén wing (AW) model suggests the generation of Alfvén wings controls the saturation of the reconnection potential [*Ridley*, 2007; *Kivelson and Ridley*, 2008]. Alfvén wings are created by Alfvén waves traveling along a magnetic field [*Ridley*, 2007, and references therein]. The bending of a magnetic field as it flows around an object in space creates an Alfvén wave, producing a cavity at an angle to the object. This angle is defined by the Alfvén Mach number or the ratio of solar wind velocity to Alfvén wave velocity. This cavity is called an Alfvén wing. The Alfvén Mach number is inversely proportional to the magnitude of the IMF, so decreasing the Alfvén Mach number increases the Alfvén wing angle. The larger the angle in an Alfvén wing, the lower its internal electric field. The Alfvén wing electric field, which is considered to be the driver of the ionospheric field, correlates with the behavior of the reconnection potential in the simulations run by *Ridley* [2007].

[8] *Ridley* [2007] also notes that this method operates irrespective of the orientation of the IMF and further states that the Alfvén Mach number must be less than 4 for any effects to occur. Full formation of Alfvén wings and full saturation effects are found when the Alfvén Mach number is less than 1 [*Ridley*, 2007]. For $V = 400$ km/s and $n = 5$ cm^{-3}, full formation of Alfvén wings (Alfvén Mach number ≤ 1) would require an IMF of greater than 40 nT. These conditions rarely occur in the solar wind, and transpolar saturation is seen in several studies at lower IMF values [*Hairston et al.*, 2003; *MacDougall and Jayachandran*, 2006; *Lopez et al.*, 2009]. Some effects could be expected for $V = 400$ km/s, $n = 5$ cm^{-3}, and an IMF of 10 nT or greater (Alfvén Mach number ≤ 4). The only further requirement for Alfvén wings is the time necessary to develop. *Ridley* [2007] estimates it takes roughly an hour for the Alfvén wave to propagate along the Alfvén wing for $V = 400$ km/s, $n = 5$ cm^{-3}, and IMF of 20 nT. Thus, for the AW model to be valid, the reconnection potential cannot saturate within an hour of the Alfvén Mach number decreasing below 4. Further, the Alfvén Mach number must remain less than 4 during saturation.

[9] The magnetosheath force balance (MFB) model explains both the linear response of the transpolar potential to the IEF for small IMF and the saturation of the transpolar potential in a single conceptual model. The MFB model treats the viscous portion of the transpolar potential as a function of solar wind speed and density, decoupling the viscous interaction from changes in the IMF. The MFB model suggests that the saturation of the reconnection potential is controlled by the relative importance of the $\boldsymbol{J} \times \boldsymbol{B}$ force in the magnetosheath (Lopez et al., submitted manuscript, 2009). The $\boldsymbol{J} \times \boldsymbol{B}$ force and the gradient of the plasma pressure are the total force exerted on plasma. The relative importance of either force can be determined from the ratio of plasma pressure to magnetic pressure (β_{ms}). During nominal solar wind conditions, the plasma pressure gradient is the dominant force in the magnetosheath ($\beta_{ms} \gg 1$). It diverts the flow around the magnetosphere producing a geoeffective length in the solar wind that is much less than the width of the magnetosphere [*Burke et al.*, 1999]. As the solar wind magnetic field increases, β_{ms} approaches 1. At that point, the $\boldsymbol{J} \times \boldsymbol{B}$ force is of comparable magnitude to the gradient of the plasma pressure, and any increase of the magnetic field in the solar wind increases the $\boldsymbol{J} \times \boldsymbol{B}$ force in the magnetosheath, causing a proportionally greater diversion of the flow around the magnetopause [*Borovsky and Denton*, 2006; *Lavraud and Borovsky*, 2008; Lopez et al., submitted manuscript, 2009].

[10] This greater diversion of the magnetosheath flow decreases the geoeffective length in the solar wind. The projection of the IEF on the extent of the solar wind flow that intersects the dayside merging line is the reconnection potential. Thus, the reconnection potential is limited even as the IMF increases, because the extent of the solar wind flow that intersects the dayside merging line decreases as the IMF increases. Thus, for the MFB model to be valid, the

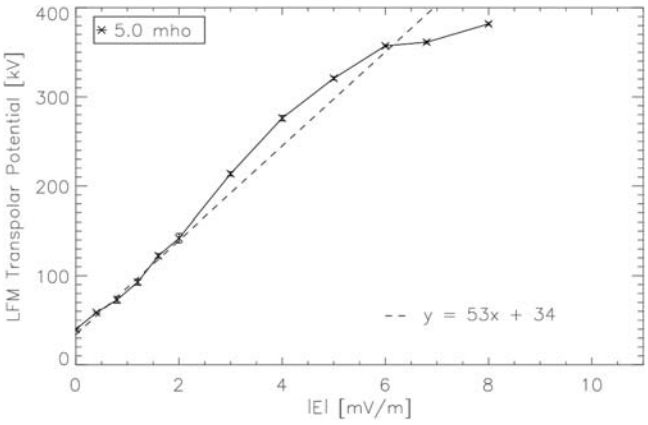

Figure 1. LFM simulated transpolar potential versus IEF (for exclusively southward IMF) for 5.0 mho conductivity. The dash line is an extrapolation of the linear regression calculated between 0.4 and 1.6 mV/m.

reconnection potential must transition to saturation as β_{ms} approaches 1 in the nose of the magnetosheath, regardless of the orientation of the IMF.

[11] This paper examines the dependence of the transpolar potential on the Y component of the IMF. In geocentric solar magnetospheric (GSM) coordinates, the X component (B_x) lies along the Sun-Earth line. The Y component (B_y) is perpendicular to the Earth's magnetic dipole along the dawn-to-dusk line. The Z component (B_z) is perpendicular to B_x and B_y, with its positive axis in the same sense as the northern magnetic field of the Earth. Most studies completed in support of the above theories have examined the transpolar potential with regard to large, negative B_z. This paper studies the response of the transpolar potential to large B_y. Beginning with a review of Lyon-Fedder-Mobarry (LFM) global MHD simulation results, the IMF dependence of the simulation results is then compared to the IMF B_y dependence of the transpolar potential determined using Defense Meteorological Satellite Program (DMSP) satellite data and Assimilative Mapping of Ionospheric Electrodynamics (AMIE) results.

2. LFM Global MHD Simulation

[12] The Lyon-Fedder-Mobarry (LFM) global MHD simulation is a three-dimensional code that models the environment around Earth by solving the single fluid, ideal MHD equations [*Lyon et al.*, 2004]. An idealized, two-dimensional ionospheric simulation is coupled to the inner boundary of the LFM simulation [e.g., *Fedder and Lyon*, 1987]. Upstream solar wind conditions and ionospheric conditions are specified by the user. Numerical diffusion facilitates simulated reconnection in the LFM.

[13] The LFM simulation was used to model the transpolar potential as a function of exclusively southward IMF (B_z) and as a function of exclusively dawn-dusk IMF (B_y). The LFM simulation was run with $V_x = -400.0$ km/s, $n = 5.0$ cm^{-3}, a sound speed of 40.00 km/s, zero dipole tilt, and a uniform ionosphere with no Hall conductivity. The Pedersen conductivity was uniform and fixed at 5.0, 10.0, or 20.0 mho. The transpolar potential was calculated by averaging the total potential difference in the northern polar cap of the ionosphere from 1400 simulation time (ST) to 1600 ST. The standard deviation was calculated for the total potential difference from 1400 ST to 1600 ST and used to estimate error in the reported values of the transpolar potential. The standard deviations were on the order of 0.0–6.0 kV; thus, they are difficult to see on some of the plots. The viscous potential was calculated by a linear regression fit for 0.4–1.6 mV/m IEF in exclusively negative B_z simulation runs. The reconnection potential was calculated by subtracting the viscous potential from the transpolar potential.

3. Simulated Response to Large B_z

[14] Simulated transpolar potentials as a function of the magnitude of the interplanetary electric field (IEF) for exclusively southward IMF are plotted in Figure 1. Because the solar wind velocity is held constant in the simulation, increasing the magnitude of the IEF is tantamount to increasing the magnitude of the southward magnetic field. The LFM simulated transpolar potential saturates for large, negative B_z.

[15] Most literature discusses the transpolar potential response as either linear or saturated. In this paper, the transpolar potential is split into three regions to allow discussion of the transition. The linear region is between 0.0 and 3.0 mV/m. The transition region, where the slope begins to flatten out and the potential becomes less sensitive to increases in the IMF, is between 3.0 and 6.0 mV/m. The saturation region is above 6.0 mV/m.

[16] In the low-IEF regime, the data are fitted using linear regression. The slope of the line has units of length with a value of 53×10^6 m ~8.3 R_E. Following Lopez et al. (submitted manuscript, 2009), we identify this length as the geoeffective length, that is to say the extent of the solar wind flow that intersects the dayside merging line in the simulation. *Burke et al.* [1999] determined a geoeffective length using DE 2 electric field observations and found it to be 4.38–4.62 R_E in the low-IEF regime, while the DMSP drift meter data give a geoeffective length of about 7.4 R_E (Lopez et al., submitted manuscript, 2009). The smaller observed geoeffective lengths compared to the simulated geoeffective lengths are consistent with the smaller observed transpolar potential compared to the simulated transpolar potential [e.g., *Lopez et al.*, 2009]. The y intercept of the line ($B_y = B_z = 0$) is interpreted to be the viscous potential for these simulated conditions (Lopez et al., submitted manuscript, 2009). The viscous potential is ~34 kV for a solar wind density of 5.0 cm^{-3} and a speed of 400.0 km/s.

[17] In the transition region, the potential begins to respond nonlinearly to the IEF. Above 4.0 mV/m, the simulated transpolar potential has a decreasing response to the IEF. This is seen through the decrease in the slope between 4.0 and 5.0 mV/m. From 3.0 to 4.0 mV/m, the simulated transpolar potential increases by ~62 kV, while from 4.0 to 5.0 mV/m, it only increases by ~45 kV. The transition in the simulated transpolar potential occurs when the potential is between 280 and 320 kV at an IEF between 4.0 and 5.0 mV/m. In the saturation region, the simulated transpolar potential reaches a maximum value of ~380 kV. The maximum transpolar potential is large compared to observations of the potential [e.g., *Lopez et al.*, 2009; Lopez

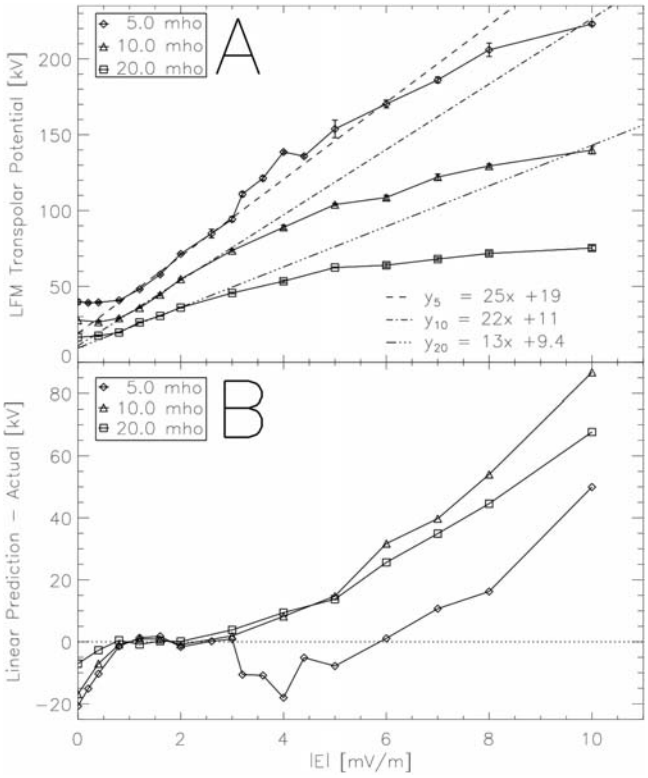

Figure 2. (a) LFM simulated transpolar potential versus IEF (for exclusively dawn-dusk IMF) for 5.0, 10.0, and 20.0 mho conductivities. The three broken lines are extrapolations of the linear regressions calculated for each run between 0.8 and 2.0 mV/m. (b) The difference between the prediction from the linear fit and the actual LFM simulated transpolar potential versus IEF for an exclusively B_y IMF for 5.0, 10.0, and 20.0 mho conductivities.

et al., submitted manuscript, 2009]. While the LFM simulation is known to overpredict the transpolar potential by 1.5–2 times, it provides accurate trends.

4. Simulated Response to Large B_y

[18] Simulated transpolar potentials as a function of the magnitude of the IEF for exclusively dawn-dusk IMF are plotted in Figure 2a. Three different values of ionospheric Pedersen conductivity were used, but for all of the simulation runs, the solar wind speed was held to a constant of 400.0 km/s in the negative × direction and the solar wind density was a constant of 5.0 cm^{-3}. Again, because the solar wind velocity is held constant in the simulation, increasing the magnitude of the IEF is tantamount to increasing the magnitude of the magnetic field. The simulation results presented in Figure 2 are computed with varying B_y. It can be seen that the LFM simulated transpolar potential saturates for large $|B_y|$.

[19] As before, the simulated transpolar potential response may be split into three regions. Each conductivity has a slightly different range for the three regions. For 5.0 mho conductivity, the linear region is between 0.0 and 3.0 mV/m, the transition region is between 3.0 and 6.0 mV/m, and the saturation region is above 6.0 mV/m. For 10.0 mho conductivity, the linear region is between 0.0 and 2.0 mV/m, the transition region is between 2.0 and 6.0 mV/m, and the saturation region is above 6.0 mV/m. For 20.0 mho conductivity, the linear region is between 0.0 and 2.0 mV/m, the transition region is between 2.0 and 5.0 mV/m, and the saturation region is above 5.0 mV/m. Saturation occurs for all three conductivities shown.

[20] In the linear region, the data are fitted using linear regression between an IEF of 0.8 and 2.0 mV/m. The slope of each line has the units of length (10^6 m). As before, the slope indicates the extent of the solar wind flow that intersects the dayside merging line in the simulation, although now the projection of the applied electric field to the tilted merging line must be considered using the formula by *Kan and Lee* [1979] and a 90° clock angle, which has been shown to be valid in a (different) global MHD simulation [*Hu et al.*, 2009]. Therefore, the simulated geoeffective length in the solar wind for 5.0 mho ionospheric conductivity is 25×10^6 m/$\sin^2(\theta/2)$, ~7.8 R_E. This is essentially the same simulated geoeffective length in the solar wind that was determined for large, negative B_z.

[21] The *y* intercept for each linear regression in B_y, which might be interpreted to be the viscous potential, is significantly smaller than the simulated transpolar potential for zero magnetic field in the solar wind or the viscous potentials reported by Lopez et al. (submitted manuscript, 2009). It is not clear what the origin of this discrepancy is. Figure 2 illustrates that the simulated transpolar potential becomes asymptotic for smaller values of B_y-dominated IEF for all conductivities. The effect of the reconnection potential is only evident when it exceeds the viscous potential. This is in marked contrast to the exclusively southward IMF cases, where the viscous potential and the reconnection potential seem to add directly to give the transpolar potential.

[22] In the transition region, the simulated transpolar potential responds nonlinearly to the IEF. Above 4.0 mV/m for 5.0 mho conductivity (3.0 mV/m for 10.0 and 20.0 mho conductivities), the simulated transpolar potential has a decreased response to an increase in the IMF magnitude. This is seen in Figure 2b, where the difference between the linear prediction and actual simulated transpolar potential versus IEF is plotted. Clearly, all of the simulated transpolar potentials are deviating from the linear response. The transition in the simulated transpolar potential with 5.0 mho ionospheric conductivity occurs when the potential is between 140 and 150 kV at an IEF between 4.0 and 5.0 mV/m. The transitions in the simulated transpolar potentials with 10.0 and 20.0 mho ionospheric conductivities occur when the potentials are between 74 and 89 mV/m and 46 and 53 mV/m, respectively, and the IEF is between 3.0 and 4.0 mV/m. In the saturation region, the simulated transpolar potential reaches a maximum value of ~210 kV for 5.0 mho conductivity, ~130 kV for 10.0 mho conductivity, and ~72 kV for 20.0 mho conductivity.

5. Observational Estimates of the Potential During Periods of Large B_y

[23] Both exclusively B_y IEF and exclusively B_z IEF cause the transpolar potential to saturate in the LFM simulation. Observations of the transpolar potential saturation for intervals of B_z-dominated IMF have been confirmed in several studies [e.g., *Russell et al.*, 2001; *Hairston et al.*,

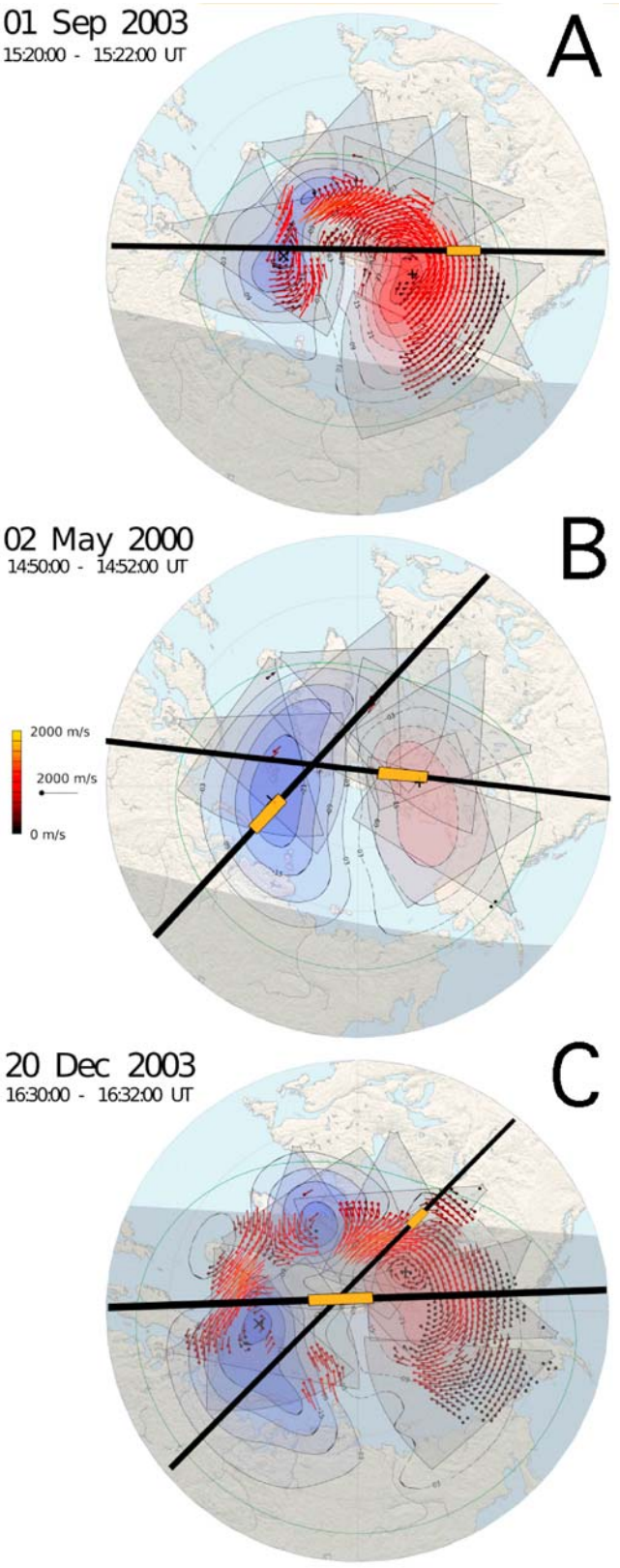

2003; *MacDougall and Jayachandran*, 2006; *Lopez et al.*, 2009]. The largest values for saturation seen in the DMSP data were ~230 kV [*Lopez et al.*, 2009]. However, no previous study has investigated whether the observed transpolar potential also saturates for large B_y-dominated IMF. To test this, 98 intervals were identified between January 1999 and December 2003. Intervals were selected if the magnitude of B_y was larger than 5.00 nT; B_z was between −1.00 and +4.00 nT with a majority of it being positive; and the B_z was mainly positive for the preceding 4 h. The corresponding 1 min Assimilative Mapping of Ionospheric Electrodynamics (AMIE) data (generously provided by Aaron Ridley) were available for the period in question. Propagated 1 min OMNI solar wind data were obtained from CDAWeb.

[24] DMSP transpolar potentials were also obtained for each interval. The Defense Meteorological Satellite Program (DMSP) has several satellites in Sun-synchronous polar orbits at ~800 km altitude. The spacecraft orbiting along the dawn-dusk synchronous path during 1999–2003 was F-13. The satellites with 0900–2100 local time nodes during 1999–2003 were F-12 and F-15. Using the drift meter data from the satellites, the potential along the pathway was calculated during the 22–26 min pass over a polar region [e.g., *Hairston et al.*, 2003]. These data are publicly available on the Web at the University of Texas at Dallas (http://cindispace.utdallas.edu/DMSP/dmsp_data_at_utdallas.html). The difference between the maximum and minimum reported values is used to calculate the transpolar potential along the DMSP orbital track. For each selected solar wind interval, any DMSP satellite pass occurring during the interval was recorded. For each pass, the IEF is averaged over the pass interval. However, how well the DMSP spacecraft potential represents the actual potential depends on how close the spacecraft came to the actual maximum and minimum of the ionospheric potential during the pass.

[25] Figure 3 contains three Super Dual Auroral Radar Network (SuperDARN) plots illustrating plasma convection in the polar region. Each plot has one or two DMSP satellite trajectories superimposed in black. The approximate location of the satellite during the 2 min interval, during which the data for the convection map was collected, is shown in yellow. The SuperDARN plots give approximate locations of the maximum (plus) and minimum (cross) polar cap potentials, and one can see that, in these DMSP passes during these periods, the estimates of the polar cap potential should be good. Table 1 lists the values of the DMSP

Figure 3. Three SuperDARN convection maps with DMSP satellite passes superimposed. The maximum (plus) and minimum (cross) polar cap potentials are marked on each map. (a) The SuperDARN convection map for 1 September 2003, between 1520 and 1522. It has an F-13 pass superimposed, with its position between 1520 and 1522 marked in yellow. (b) The SuperDARN convection map for 2 May 2000, between 1450 and 1452. It has an F-13 and an F-15 pass superimposed, with each satellite position between 1450 and 1452 marked in yellow. (c) The SuperDARN convection map for 20 December 2003, between 1630 and 1632. It has an F-13 and an F-15 pass superimposed, with each satellite position between 1630 and 1632 marked in yellow.

Table 1. Measurements by DMSP Satellites During Selected Intervals of B_y-Dominant IMF[a]

Year	Month	Day	Sat.	Start	End	Max Pot	Min Pot	DMSP Trans. Pot.	Avg AMIE Trans. Pot.	Avg B_y	Avg $\|E_t\|$
2003	9	1	F13	1506	1530	43.0	−32.4	75.4	77.7	−8.37	3.95
2000	5	2	F13	1439	1503	70.1	−32.6	103	92.4	−11.27	7.46
2000	5	2	F15	1443	1509	7.6	−38.7	46.3	93.2	−11.23	7.41
2003	12	20	F15	1616	1642	57.8	−41.3	99.1	82.4	−14.96	8.15
2003	12	20	F13	1619	1643	49.0	−51.6	101	85.1	−14.39	8.08

[a]Average AMIE, B_y, and $|E_t|$ for the same selected intervals. Max Pot = maximum potential; Min Pot = minimum potential; Trans. Pot. = transpolar potential.

maximum and minimum potentials and the transpolar potential, as well as the average AMIE transpolar potential, B_y, and transverse IEF for the same interval.

[26] For 1 September 2003, the DMSP F-13 satellite passes near both the maximum and minimum potentials, as given by SuperDARN (Figure 3a). The DMSP transpolar potential for this pass is 75.5 kV. For 2 May 2000, the DMSP F-13 satellite passes over the reported maximum potential ($DMSP_{maximum}$ = 70.1 kV) while the DMSP F-15 satellite passes over the reported minimum potential ($DMSP_{minimum}$ = −38.7 kV) (Figure 3b). The DMSP F-13 transpolar potential for this pass is 103 kV. For 20 December 2003, the DMSP F-13 and F-15 satellites pass near both the maximum and minimum potentials (Figure 3c). For this pass, the DMSP F-13 transpolar potential is 101 kV and the DMSP F-15 transpolar potential is 99.2 kV. Comparing the DMSP transpolar potentials and their average B_y, the change from 75.5 to 103 kV corresponds to a change in the average solar wind B_y from −8.37 nT to approximately −11.25 nT. So comparing the 1 September 2003 pass to the 2 May 2000 pass, there is a 27 kV difference in ionospheric potential corresponding to a 2.88 nT difference in the average solar wind B_y. In contrast, comparing the 2 May 2000 pass (103 kV) to the 20 December 2003 pass (101 kV), there is a −2 kV difference in potential for a 3.43 nT difference in the average B_y. These three cases suggest saturation of the potential for large B_y, although other reasons might be suggested for these changes if the incidents were isolated.

[27] Considering a larger sample size, the DMSP transpolar potentials are plotted as a function of the transverse IEF and maximum AMIE transpolar potentials are plotted as a function of 1 mV/m bins of transverse IEF in Figure 4. The 10,301 min of AMIE data are sorted by corresponding transverse IEF and separated into 1 mV/m bins. The diamonds in Figure 4 indicate the maximum AMIE transpolar potentials as a function of their transverse IEF bins. Clearly, the maximum AMIE transpolar potentials saturate. The bars in Figure 4 plot the 105 DMSP F-13 transpolar potentials as a function of their average transverse IEF. The DMSP transpolar potential stays within the envelope of maximum AMIE transpolar potential. The low potential values in the DMSP data are from passes where the satellites did not enter the regions of highest or lowest potential due to the skewing of the polar cap by B_y-dominated IMF [*Heppner*, 1977]. The DMSP transpolar potentials also show a trend for saturation, although the number of passes at the higher transverse IEF is low.

[28] The evidence is clear: the transpolar potential saturates for sufficiently large-magnitude B_y-dominated IEF. The transition from a linear dependence on transverse IEF to a saturated potential occurs between 4 and 5 mV/m, as seen in Figure 4. The maximum transpolar potential is 114 kV for AMIE data and 103 kV for DMSP data. Both values are between half and two-thirds the simulated transpolar potential for 5.0 mho conductivity, which is the approximate scaling between the LFM potentials and observed potentials for dominantly southward IMF.

6. Discussion

[29] Transpolar potential saturation has been shown in each of the three cases above: simulated B_z-dominated IEF, simulated B_y-dominated IEF, and observed B_y-dominated IEF. Returning to the explanations of transpolar potential saturation, the results are considered with respect to the R1 model, AW model, and MFB model.

[30] The R1 model predicts the saturation of the transpolar potential to occur at the same potential value for any given IEF if conductivity, solar wind density, and solar wind velocity all have the same value. This prediction may be verified using the LFM simulation results with 5.0 mho conductivity. In the exclusively B_z IEF case, the simulated transpolar potential becomes nonlinear between 4.0 and 5.0 mV/m at 280–320 kV. In the exclusively B_y IEF case, the simulated transpolar potential becomes nonlinear between 4.0 and 5.0 mV/m at 140–150 kV. Therefore, according to Ohm's law, the current generated in one case is different from the other case. It cannot be the current that limits the transpolar potential, since these examples represent significantly different values of the Region 1 current.

[31] This is not to say the Region 1 current does not affect the reconnection potential. The Region 1 current does affect

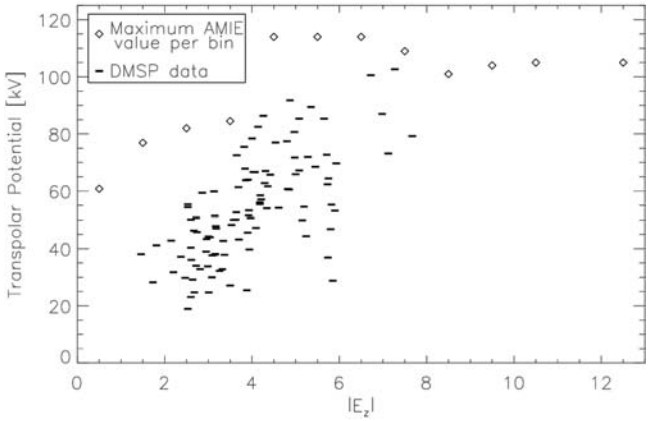

Figure 4. Maximum AMIE transpolar potential (diamonds) for each 1 mV/m bin versus 1 mV/m bins of B_y-dominant transverse IEF and DMSP transpolar potentials (dashes) versus B_y-dominant transverse IEF.

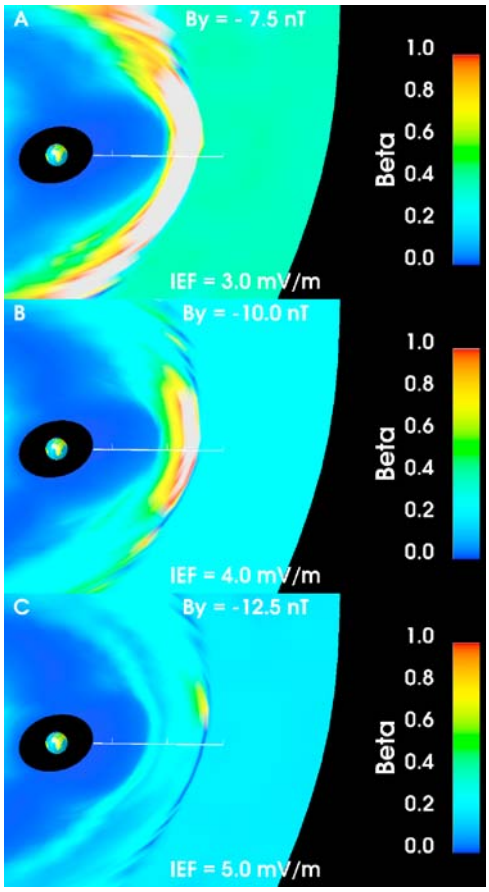

Figure 5. LFM-simulated β for 5.0 mho conductivity mapped to a plane tilted 45° from the North Pole toward dusk and perpendicular to the expected merging line. The scale is from 0 to 1; gray indicates β greater than 1. The white line indicates the positive x axis from 3 to 15 R_E with tick marks at 5, 10, and 15 R_E. (a) Solar wind $B_y = -7.5$ nT and IEF = 3.0 mV/m. (b) Solar wind $B_y = -10.0$ nT and IEF = 4.0 mV/m. (c) Solar wind $B_y = -12.5$ nT and IEF = 5.0 mV/m.

the shape of the magnetopause and the thickness of the magnetosheath. Figures 5 and 6 depict a plane of the magnetosheath tilted 45° from the North Pole toward the dusk side of the Earth for the 5.0 and 20.0 mho conductivity cases, respectively. Examining Figures 5c and 6c, the magnetosheath for the 20.0 mho case (Figure 6) is thicker and blunter than the 5.0 mho case (Figure 5). This thickening and blunting occurs through erosion of the magnetic field on the dayside. The increased conductivity, even with slightly smaller transpolar potentials, provides an increased current, which erodes the dayside magnetic field as suggested by *Siscoe et al.* [2004]. *Merkin et al* [2005] and Lopez et al. (submitted manuscript, 2009) suggest that greater erosion provides a larger region of magnetosheath over which the plasma flow may be diverted, thereby shortening the extent of the solar wind flow that intersects with the merging line.

[32] The AW model predicts the saturation of the transpolar potential to occur after an hour of low Alfvén mach number (<4) while the Alfvén Mach number remains less than 4. An Alfvén Mach number of 4 occurs for a solar wind velocity of 400 km/s, a solar wind density of 5 cm^{-3}, and an IMF of 10 nT. The concurrent IEF is 4 mV/m, which is close to the value where the simulated transpolar potentials begin to respond nonlinearly. However, for the event on 20 December 2003 presented in Figure 3, the average Alfvén Mach number (5.2) was greater than 4 and the solar wind was not steady for an hour to allow the formation of the Alfvén wing. Yet the event is an example of a saturated potential. Thus, this study finds no strong evidence in favor of the AW model. Moreover, the AW model does not explain why only a fraction of the electric field in the Alfvén wing is actually communicated to the ionosphere. *Ridley* [2007] suggests that only 10% of the length of the dayside magnetopause is undergoing reconnection, but *Borovsky et al.* [2008] presents evidence that dayside merging occurs in the BATSRUS simulation code over a much greater extent.

[33] The MFB model predicts the saturation of the transpolar potential to occur as β_{ms} approaches 1 at the nose of the magnetosheath, and it also explains why even for small

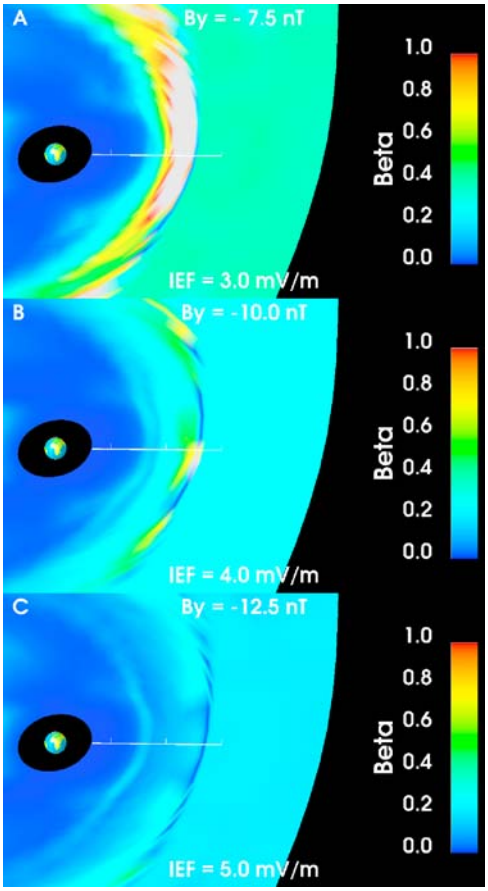

Figure 6. LFM-simulated β for 20.0 mho conductivity mapped to a plane tilted 45° from the North Pole toward dusk and perpendicular to the expected merging line. The scale is from 0 to 1; gray indicates β greater than 1. The white line indicates the positive x axis from 3 to 15 R_E with tick marks at 5, 10, and 15 R_E. (a) Solar wind $B_y = -7.5$ nT and IEF = 3.0 mV/m. (b) Solar wind $B_y = -10.0$ nT and IEF = 4.0 mV/m. (c) Solar wind $B_y = -12.5$ nT and IEF = 5.0 mV/m.

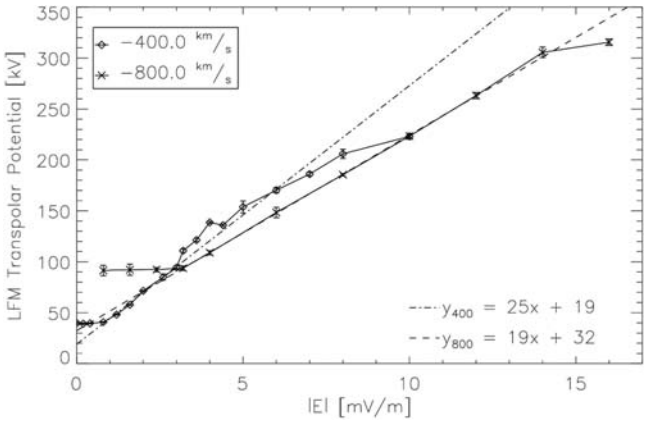

Figure 7. LFM-simulated transpolar potential versus exclusively B_y IEF for 5.0 mho conductivity and solar wind V_x = −400.0 and −800.0 km/s. The broken lines are extrapolations of the linear regression calculated between 0.4 and 1.6 mV/m for V_x = −400.0 km/s and between 3.2 and 8.0 mV/m for V_x = −800.0 km/s.

IMF values the total potential drop across the width of the magnetosphere is not imposed on the ionosphere. In the simulations using exclusively B_y IEF, the 5.0 mho conductivity simulated transpolar potential becomes nonlinear between 4.0 and 5.0 mV/m, or 10.0 and 12.5 nT. Figure 5 depicts three planes tilted 45° from the North Pole toward dusk in which β_{ms} has been plotted. These planes are normal to the expected merging line [*Moore et al.*, 2002]. All three images are from the same simulation time in the runs of 5.0 mho conductivity; only the magnitude of B_y has changed in each. The color bar is set between 0 and 1; the gray areas are β_{ms} greater than 1. Figure 5a has a B_y of −7.5 nT, corresponding to an IEF of 3.0 mV/m. β_{ms} is clearly greater than 1 for a large area of the magnetosheath. Figure 5b has a B_y of −10.0 nT, corresponding to an IEF of 4.0 mV/m. β_{ms} is greater than 1 at the nose of the magnetosheath but does not extend into the flanks. Figure 5c has a B_y of −12.5 nT, corresponding to an IEF of 5.0 mV/m. β_{ms} is less than 1 throughout the magnetosheath. These results support the MFB prediction of magnetosheath behavior during the transition from linear to nonlinear responses in the transpolar potential. Figure 6 follows the same structure as Figure 5 for the 20.0 mho conductivity case and provides additional support to the MFB model. In the exclusively B_y IEF simulated cases, the 20.0 mho conductivity simulated transpolar potential becomes nonlinear between 3.0 and 4.0 mV/m or 7.5 and 10.0 nT. Again, the β_{ms} is greater than 1 for −7.5 nT (3.0 mV/m), but it reaches 1 at approximately −10.0 nT (4.0 mV/m) and is much less than 1 by −12.5 nT (5.0 mV/m).

[34] The MFB model appears to be predictive for both B_y-dominant IEF and B_z-dominant IEF. The difference in the two IEF cases is in the geometry of the dayside merging line. The geometry of the B_y-dominant IMF dayside merging region is more complicated than the geometry of the B_z-dominant IMF dayside merging region [*Moore et al.*, 2002]. The B_y-dominant IMF merging line is expected to cross the nose of magnetopause at a 45° angle, going from pole to pole, partially encircling the cusp regions. This geometry is captured by the *Kan and Lee* [1979] clock angle dependence, which has been shown to correctly predict the reconnection potential in other simulations [*Hu et al.*, 2009]. Incorporating this factor, we find that the simulated geoeffective length in the solar wind is the same for exclusively southward as well as dawn-dusk orientations for the same solar wind conditions. This adds support to the argument that the geoeffective length is established by the forces in the magnetosheath diverting flow from the dayside merging line.

[35] In addition, a brief examination of the role of solar wind speed in establishing the potential lends strong support to the MFB model. Figure 7 is a plot of the simulated transpolar potential for solar wind speeds of 400.0 and 800.0 km/s. Doubling the solar wind speed changes the asymptotic behavior in the linear regime. The total potential does not rise above the viscous value until the reconnection portion of the potential is larger than the viscous value. This behavior merits further investigation, but that is beyond the scope of this paper.

[36] While the viscous potential increases with increasing solar wind speed, the simulated geoeffective length (19 ×

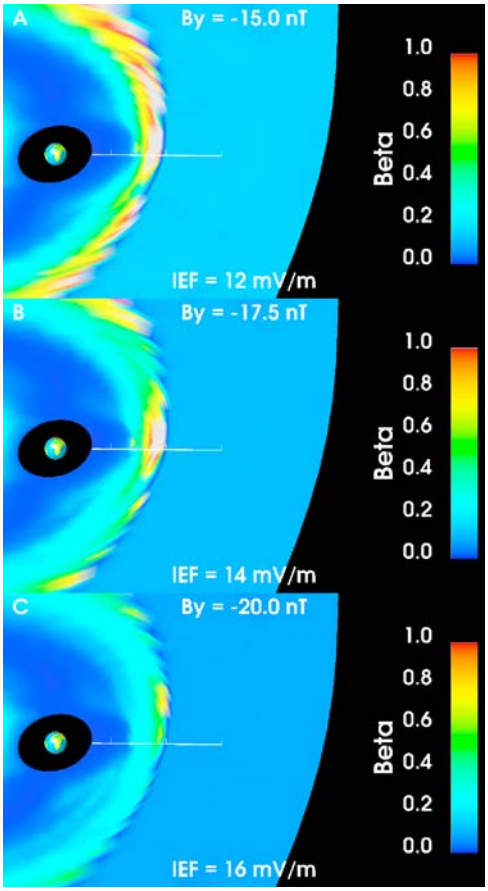

Figure 8. LFM-simulated β for 5 mho conductivity and solar wind V_x = −800.0 km/s mapped to a plane tilted 45° from the North Pole toward dusk and perpendicular to the expected merging line. The scale is from 0 to 1; gray indicates β greater than 1. The white line indicates the positive x axis from 3 to 15 R_E with tick marks at 5, 10, and 15 R_E. (a) B_y = −15.0 nT and IEF = 12. mV/m. (b) B_y = −17.5 nT and IEF = 14. mV/m. (c) B_y = −20.0 nT and IEF = 16. mV/m.

10^6 m/sin^2 (θ/2), ~6.0 R_E) in the linear regime decreases so that the reconnection potential is fairly independent of velocity. It has been shown to be consistent with the MFB model since a larger solar wind velocity produces larger magnetosheath plasma pressures and gradient, thus producing a greater diversion of the magnetosheath flow and a smaller geoeffective length in the solar wind. Doubling the solar wind speed also extends the linear regime due to the increase in the magnetosheath plasma pressure. Figure 8 presents the β for the 800.0 km/s case in Figure 7. As can be seen, β across the magnetosheath is larger for larger solar wind speed, and the behavior of the potential (not saturating until a larger IMF is reached) is consistent with the larger β.

7. Conclusions

[37] This study examined the response of the transpolar potential to B_y-dominant IEF. Saturation of the transpolar potential was found in both simulation results and observations. The DMSP data and AMIE results confirm the LFM simulation prediction. The transpolar potential saturates for B_y-dominant IEF. The value of the saturation potential is consistent with the *Kan and Lee* [1979] reconnection electric field and the same simulated geoeffective length found for exclusively southward IMF by Lopez et al. (submitted manuscript, 2009). Of the models examined, the results seem to be most consistent with the magnetosheath force balance model.

[38] **Acknowledgments.** The authors acknowledge fruitful conversations with G.L. Siscoe, A.J. Ridley, and J. Borovsky during the 2009 GEM workshop in Snowmass, CO. This material is based upon work supported by CISM, which is funded by the STC Program of the National Science Foundation under agreement ATM-0120950, as well as work supported by NASA grants NNX09AI63G and 4200254162ESAX22008D and NSF grant ATM-0900920.

[39] Masaki Fujimoto thanks Patrick Newell and another reviewer for their assistance in evaluating this paper.

References

Axford, W. I., and C. O. Hines (1961), A unifying theory of high-latitude geophysical phenomena and geomagnetic storms, *Can. J. Phys.*, *39*, 1433–1464.

Boyle, C. B., P. H. Reiff, and M. R. Hairston (1997), Empirical polar cap potentials, *J. Geophys. Res.*, *102*(A1), 111–125, doi:10.1029/96JA01742.

Borovsky, J. E., and M. H. Denton (2006), Differences between CME-driven storms and CIR-driven storms, *J. Geophys. Res.*, *111*, A07S08, doi:10.1029/2005JA011447.

Borovsky, J. E., M. Hesse, J. Birn, and M. M. Kuznetsova (2008), What determines the reconnection rate at the dayside magnetosphere?, *J. Geophys. Res.*, *113*, A07210, doi:10.1029/2007JA012645

Burke, W. J., D. R. Weimer, and N. C. Maynard (1999), Geoeffective interplanetary scale sizes derived from regression analysis of polar cap potentials, *J. Geophys. Res.*, *104*(A5), 9989–9994, doi:10.1029/1999JA900031.

Cowley, S. W. H. (1982), The causes of convection in the Earth's magnetosphere: A review of developments during the IMS, *Rev. Geophys.*, *20*(3), 531–565.

Dungey, J. W. (1961), Interplanetary magnetic field and the auroral zones, *Phys. Rev. Lett.*, *6*, 47–49.

Fedder, J. A., and J. G. Lyon (1987), The solar wind-magnetosphere-ionosphere current-voltage relationship, *Geophys. Res. Lett.*, *14*(8), 880–883.

Hairston, M. R., T. W. Hill, and R. A. Heelis (2003), Observed saturation of the ionospheric polar cap potential during the 31 March 2001 storm, *Geophys. Res. Lett.*, *30*(6), 1325, doi:10.1029/2002GL015894.

Heppner, J. P. (1977), Empirical models of high-latitude electric fields, *J. Geophys. Res.*, *82*(7), 1115–1125.

Hu, Y. Q., Z. Peng, C. Wang, and J. R. Kan (2009), Magnetic merging line and reconnection voltage versus IMF clock angle: Results from global MHD simulations, *J. Geophys. Res.*, *114*, A08220, doi:10.1029/2009JA014118.

Kan, J. R., and L. C. Lee (1979), Energy coupling function and solar wind magnetosphere dynamo, *Geophys. Res. Lett.*, *6*(7), 577–580.

Kivelson, M. G., and A. J. Ridley (2008), Saturation of the polar cap potential: Inference from Alfvén wing arguments, *J. Geophys. Res.*, *113*, A05214, doi:10.1029/2007JA012302.

Lavraud, B., and J. E. Borovsky (2008), Altered solar wind-magnetosphere interaction at low Mach numbers: Coronal mass ejections, *J. Geophys. Res.*, *113*, A00B08, doi:10.1029/2008JA013192.

Lopez, R. E., M. Wiltberger, S. Hernandez, and J. G. Lyon (2004), Solar wind density control of energy transfer to the magnetosphere, *Geophys. Res. Lett.*, *31*, L08804, doi:10.1029/2003GL018780.

Lopez, R. E., J. G. Lyon, E. Mitchell, R. Bruntz, V. G. Merkin, S. Brogl, F. Toffoletto, and M. Wiltberger (2009), Why doesn't the ring current injection rate saturate?, *J. Geophys. Res.*, *114*, A02204, doi:10.1029/2008JA013141.

Lyon, J. G., J. A. Fedder, and C. M. Mobarry (2004), The Lyon-Fedder-Mobarry (LFM) global MHD magnetospheric simulation code, *J. Atmos. Sol.-Terr. Phys.*, *66*, 1333–1350, doi:10.1016/j.jastp.2004.03.020.

MacDougall, J. W., and P. T. Jayachandran (2006), Polar cap voltage saturation, *J. Geophys. Res.*, *111*, A12306, doi:10.1029/2006JA011741.

Merkin, V. G., A. S. Sharma, K. Papadopoulos, G. Milikh, J. Lyon, and C. Goodrich (2005), Global MHD simulations of the strongly driven magnetosphere: Modeling of the transpolar potential saturation, *J. Geophys. Res.*, *110*, A09203, doi:10.1029/2004JA010993.

Moore, T. E., M.-C. Fok, and M. O. Chandler (2002), The dayside reconnection X line, *J. Geophys. Res.*, *107*(A10), 1332, doi:10.1029/2002JA009381.

Newell, P. T., T. Sotirelis, K. Liou, and F. J. Rich (2008), Pairs of solar wind-magnetosphere coupling functions: Combining a merging term with a viscous term works best, *J. Geophys. Res.*, *113*, A04218, doi:10.1029/2007JA012825.

Ober, D. M., N. C. Maynard, and W. J. Burke (2003), Testing the Hill model of transpolar potential saturation, *J. Geophys. Res.*, *108*(A12), 1467, doi:10.1029/2003JA010154.

Reiff, P. H., and J. G. Luhmann (1986), Solar wind control of the polar-cap voltage, in *Solar Wind-Magnetosphere Coupling*, edited by Y. Kamide and J. A. Slavin, pp. 453–476, Terra Sci., Tokyo.

Reiff, P. H., R. W. Spiro, and T. W. Hill (1981), Dependence of polar cap potential drop on interplanetary parameters, *J. Geophys. Res.*, *86*(A9), 7639–7648.

Ridley, A. J. (2007), Alfvén wings at Earth's magnetosphere under strong interplanetary magnetic field, *Ann. Geophys.*, *25*, 533–542.

Russell, C. T., J. G. Luhmann, and G. Lu (2001), Nonlinear response of the polar ionosphere to large values of the interplanetary electric field, *J. Geophys. Res.*, *106*(A9), 18,495–18,504.

Siscoe, G. L., G. M. Erickson, B. U. Ö. Sonnerup, N. C. Maynard, J. A. Schoendorf, K. D. Siebert, D. R. Weimer, W. W. White, and G. R. Wilson (2002a), Hill model of transpolar potential saturation: Comparisons with MHD simulations, *J. Geophys. Res.*, *107*(A6), 1075, doi:10.1029/2001JA000109.

Siscoe, G. L., N. U. Crooker, and K. D. Siebert (2002b), Transpolar potential saturation: Roles of region 1 current system and solar wind ram pressure, *J. Geophys. Res.*, *107*(A10), 1321, doi:10.1029/2001JA009176.

Siscoe, G., J. Raeder, and A. J. Ridley (2004), Transpolar potential saturation models compared, *J. Geophys. Res.*, *109*, A09203, doi:10.1029/2003JA010318.

Sonnerup, B. U. Ö., K. D. Siebert, W. W. White, D. R. Weimer, N. C. Maynard, J. A. Schoendorf, G. R. Wilson, G. L. Siscoe, and G. M. Erickson (2001), Simulations of the magnetosphere for zero interplanetary magnetic field: The ground state, *J. Geophys. Res.*, *106*(A12), 29,419–29,434.

R. C. Allen, R. J. Bruntz, S. J. Cockrell, R. E. Lopez, E. J. Mitchell, and P. L. Whittlesey, Department of Physics, University of Texas at Arlington, 502 Yates St., Box 19059, Arlington, TX 76019, USA. (mitchell@uta.edu)

J. G. Lyon, Department of Physics and Astronomy, Dartmouth College, Hanover, NH 03755, USA.

M. Wiltberger, High Altitude Observatory, National Center for Atmospheric Research, 3450 Mitchel Ln., Boulder, CO 80301, USA.